Diffuse X-ray scattering and the anomalous soft mode in NaNO$_3$

View the table of contents for this issue, or go to the journal homepage for more

Diffuse x-ray scattering and the anomalous soft mode in NaNO₃

M J Harris

Oxford Physics, Clarendon Laboratory, Parks Road, Oxford OX1 3PU, UK

Abstract. Triple-axis x-ray scattering measurements of diffuse scattering in NaNO₃ are described. NaNO₃ undergoes a structural phase transition at 549 K which results in the appearance of a superlattice reflection at the Z-point of the high-temperature Brillouin zone. However, strong diffuse scattering was observed in the low-temperature phase at $(2.5\,0\,\bar{2})$, which is a zone boundary F-point of the high-temperature phase. The temperature dependence of the diffuse scattering was measured between 295 K and 538 K. The scattering was observed to take the form of a ridge between Γ-points, and is linked with the partial softening of a transverse acoustic branch about the F-point. Using these results, an approximate determination of the magnitudes of the soft-mode eigenvectors was achieved. The observed behaviour is discussed in terms of the possibility of non-critical fluctuations into a monoclinic ordered structure, and is compared with the superficially similar behaviour of calcite (CaCO₃).

1. Introduction

At 549 K sodium nitrate (NaNO₃) undergoes a structural phase transition from the low-temperature R3̄c form to a high-temperature form with space group R3̄m. This symmetry change is marked by the appearance of superlattice reflections at the Z-points of the Brillouin zone of the high-temperature phase, and is attributed to rotational disordering of the molecular nitrate groups by 60° flips about the trigonal threefold axes. A great deal of theoretical and experimental work has been performed on this system because it is a model example of a material with mixed ionic/covalent atomic interactions, and also because a similar phase transition occurs in the isostructural mineral calcite (CaCO₃), which is of considerable geological interest.

The majority of experimental investigations have been concerned with the lattice dynamics of the phase transition, particularly using Raman spectroscopy [1–5], but also infrared spectroscopy [6, 7] and molecular dynamics simulations [8]. These authors have emphasized the importance of short-range order in determining the character of the transition, but a number of unanswered questions still remain. In particular, the reason why the phase transitions in both NaNO₃ and calcite are close to tricritical in character is not known, together with an explanation for why, in NaNO₃ alone, the critical exponent β changes from its tricritical value of 0.25 to the value 0.22 between about 450 K and T_c [9, 10].

In an attempt to answer these questions, recent work has centred on the hypothetical existence of a non-critical monoclinic phase. This phase is thought somehow to be associated with a partial softening of the transverse acoustic branch around the zone boundary F-point, which has been observed using inelastic neutron scattering [11–13]. It is also thought to be responsible for anomalies observed in the infrared spectrum close to T_c [7]. Calcite contains a similar softening, together with a unique column of inelastic scattering at the

F-point which extends in energy up to the softening transverse acoustic mode [14, 15]. This column of scattering has not been observed in $NaNO_3$ [12, 13]. At this point, it should be emphasized that all mention of 'the *F*-point' in this paper refers to the *F*-point relative to the high-temperature Brillouin zone, and not the low-temperature zone unless otherwise stated. Figure 1 shows the relationship of these *F*-points to the low-temperature Γ-points.
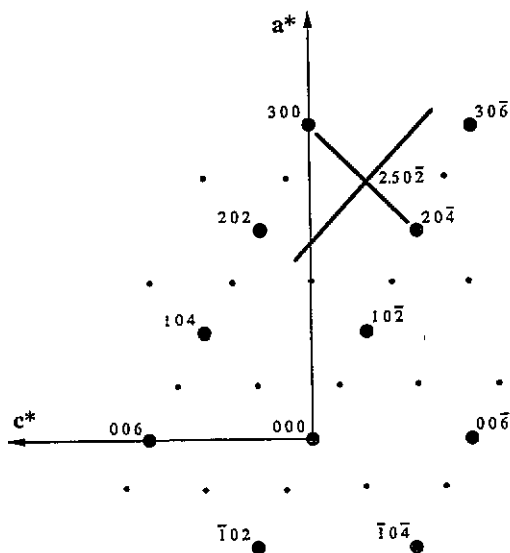

Figure 1. The a^*-c^* plane of reciprocal space for $NaNO_3$, with some of the Bragg points of the low-temperature phase labelled. The large filled circles represent Bragg reflections, and the small circles represent *F*-points of the high-temperature Brillouin zone. The axes are shown for the low-temperature form (in the high-temperature form a^* is reversed), and the heavy full lines mark the trajectories of the scans performed around the $(2.50\bar{2})$ *F*-point in the experiments.

In a molecular dynamics simulation of the phase transition in $NaNO_3$, Lynden-Bell and co-workers [8] observed high-amplitude fluctuations at the *F*-point, which led them to suggest that two major ordering processes compete in $NaNO_3$, one of which is the conventional ordering process resulting in the symmetry change $R\bar{3}m \rightarrow R\bar{3}c$ at 549 K. The alternative ordering scheme is one in which anions in planes perpendicular to the $\Gamma-F$ directions of the $R\bar{3}m$ lattice have the same orientations (rather than those perpendicular to the *c* axis as in the $R\bar{3}c$ structure), producing a monoclinic $P2/a$ structure [14] where the *F*-points become reciprocal lattice vectors. In this context, x-ray diffuse scattering has been observed (using photographic techniques) in calcite at room temperature [16] and in $NaNO_3$ close to T_c [16, 17].

In order to investigate the wavevector- and temperature-dependence of this diffuse scattering in $NaNO_3$ more precisely, x-ray scattering experiments were performed using a triple-axis diffractometer, which are reported here.

2. Experimental details

The x-ray scattering experiments were performed with a Huber two-circle diffractometer in the triple-axis configuration and Cu Kα radiation from a Stoe rotating anode source operating at 6 kW. Flat pyrolytic graphite crystals were used for the monochromator and analyser, which provided a resolution of approximately 0.01Å^{-1} in the scattering plane and 0.1 Å^{-1} perpendicular to it [18].

The single crystal of $NaNO_3$ used in the experiments was grown from an aqueous solution of analytical grade reagents and had good (104) faces. A (100) slice,

approximately 1 mm thick, was cut from the crystal and mounted on a copper block in contact with a cylindrical platinum-wound heater inside an evacuated furnace. The temperature was measured using a platinum resistance-thermometer placed inside the copper block. As the thermal expansion of $NaNO_3$ along the c axis is so large, it was found that the actual crystal temperature could be calibrated by comparing the measured c lattice parameter with the accurate lattice parameter measurements of Reeder and co-workers [19], resulting in an overall precision of about ± 1 K. The measurements were performed in reflection geometry, with the $a^* - c^*$ axes in the scattering plane. The hexagonal axial setting was used throughout the experiment and subsequent analysis, but the fact that the lattice is actually rhombohedral results in systematic absences of the form $-h + k + \ell = 3n$.

Measurements were performed for the sample temperatures 295, 368, 415, 463, 488, 512, 523, 532 and 538 K and consisted of linear scans through the F-point at $(2.5\,0\,\bar{2})$: along the $\Gamma-F$ direction and perpendicular to it, i.e. along the zone boundary. These latter scans were actually made along the $[\bar{2}\,0\,7]$ reciprocal lattice direction, which is not quite perpendicular to $\Gamma-F$: there is a discrepancy of about $1.3°$. The two trajectories used are shown in figure 1. Diffuse intensity occurs at other F-points as well, such that there is a ridge of F-point scattering along the $\Gamma-F$ direction which passes through $(3\,0\,0)$, $(4\,0\,4)$ and $(2\,0\,\bar{4})$ [16], but the strongest scattering occurs at $(2.5\,0\,\bar{2})$.

The $R\bar{3}m \rightarrow R\bar{3}c$ phase transition results in a superlattice reflection, which appears at the Z-point of the high-temperature Brillouin zone. However, this cannot be observed in the a^*-c^* setting used in this experiment because of the presence of a c-glide plane in the space group which results in a vanishing structure factor for this setting.

Deterioration of crystal quality can be a problem in high-temperature experimental studies of $NaNO_3$, possibly because the melting temperature is only about 25 K above T_c, so sample rocking curves of the Bragg peaks $(3\,0\,0)$, $(3\,0\,12)$ and $(4\,0\,4)$ were measured at each temperature to check for this. It was found that above 540 K the deterioration was such that the Bragg peaks were split into several components, indicating a progressive break-up of the crystal into misaligned mosaic blocks. The angular spread of these Bragg peaks due to the increased mosaic spread was as great as $0.5°$ at the highest temperatures. Hence, although scans were performed above 538 K, the data were considered unreliable and were not analysed.

3. Experimental results

3.1. The scattering cross section

Considering just the softening (but non-critical) phonon at the F-point in the high-temperature approximation, the x-ray scattering cross section for a wavevector transfer Q is given by [20]

$$S(Q) = \sum_q F(Q, q) g(q) F(-Q, -q) \delta(Q - G_F - q) \tag{1}$$

where q is the reduced wavevector which is defined here so that $q = 0$ at the F-point, and the term $\delta(Q - G_F - q)$ is the Dirac delta function which ensures wavevector conservation for the F-point, G_F. The static pair correlation function, $g(q)$, is given by the dynamic pair correlation function

$$g(q) = \int_{-\infty}^{\infty} d\omega \, g(q, \omega) \tag{2}$$

and is related to the static susceptibility by

$$\frac{g(q)}{k_B T} = \chi(q). \tag{3}$$

The one-phonon structure factor, $F(Q, q)$, is given as

$$F(Q, q) = \sum_n m_n^{-1/2} f_n(Q) Q \cdot e_n(q) \exp[i(Q - q) \cdot r_n] \exp(-W_n) \tag{4}$$

where the sum is over all n atoms in the unit cell, each of which has a mass m_n, a position vector r_n, an eigenvector $e_n(q)$, an atomic scattering factor $f_n(Q)$, and a Debye–Waller factor W_n. Generally speaking, the frequency of the soft mode at the F-point can be expanded as a power series about $q = 0$, so that to the second order it is given as

$$\omega^2(q, T) = \omega_0^2(T) + \sum_\alpha \varepsilon_\alpha q_\alpha^2 = \frac{k_B T}{g(q)} \tag{5}$$

where $\alpha = x, y, z$ and the parameters ε_α characterize the steepness of the phonon dispersion at the F-point. Combining the above expressions for $S(Q)$ gives

$$S(Q) = k_B T \sum_q \frac{|F(G_F, q)|^2}{\omega_0^2(T) + \sum_\alpha \varepsilon_\alpha q_\alpha^2} \delta(Q - G_F - q). \tag{6}$$

From this expression it may be expected that the diffuse scattering due to a soft phonon at the F-point has a Lorentzian distribution with respect to the reduced wavevector q. Neutron scattering measurements [12, 13] have shown that below about 500 K the soft transverse acoustic branch in NaNO$_3$ has a very flat dispersion along the Γ–F direction (figure 2). Hence, it is unclear whether expression (5) is entirely appropriate for analysing the Γ–F scans below about 500 K rather than some other more general expression. However, for consistency, it was decided that all of the x-ray diffuse scattering centred on the F-point would be analysed with a Lorentzian lineshape.
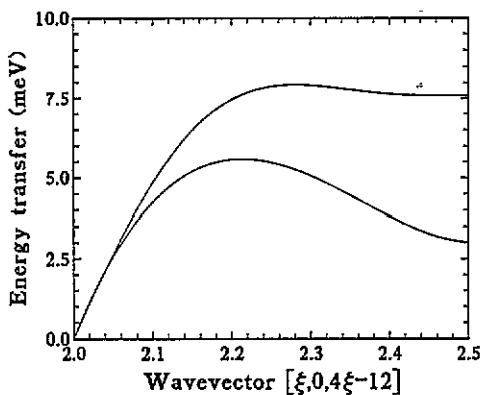

Figure 2. Schematic dispersion curves for the transverse acoustic branch along the Γ–F direction in NaNO$_3$, at 293 K (higher curve), and 553 K (lower curve), showing softening around the zone boundary F-point (where $\xi = 2.5$).
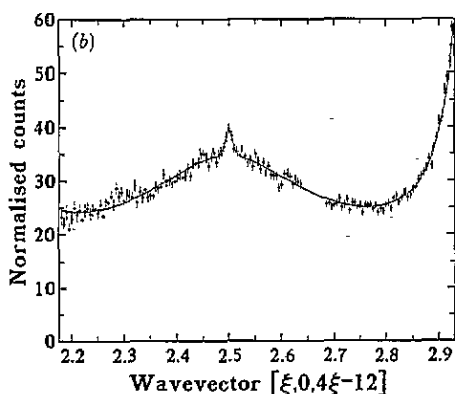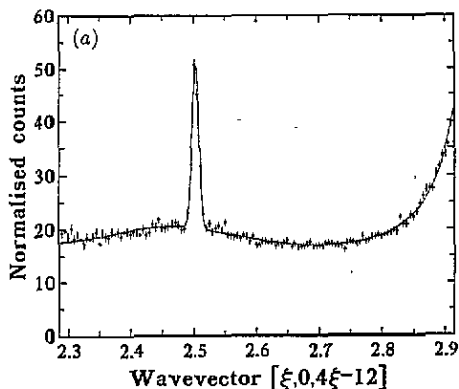
Figure 3. $\Gamma\text{--}F$ scans through the $(2.5\,0\,\bar{2})$ F-point (where $\xi = 2.5$), at temperatures of (*a*) 295 K, and (*b*) 488 K. The full curve represents the fitted profile. The data around $\xi = 2.65$ are not included in (*b*) due to the presence of a very sharp powder line from the copper mount, which appeared in most scans.
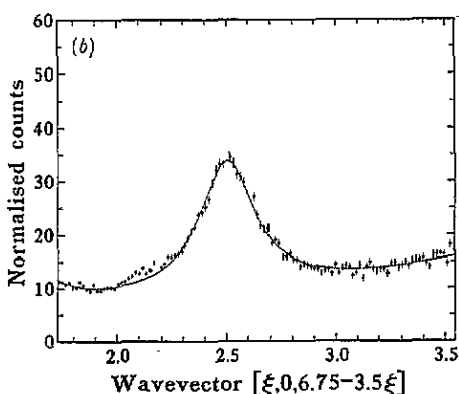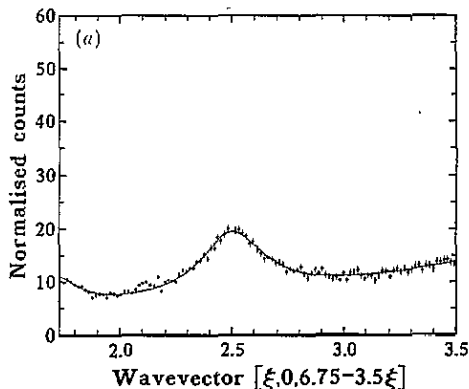
Figure 4. Scans perpendicular to the $\Gamma\text{--}F$ direction through the $(2.5\,0\,\bar{2})$ F-point (where $\xi = 2.5$), at temperatures of (*a*) 295 K, and (*b*) 488 K. The full curve represents the fitted profile to the data.

3.2. The F-point diffuse scattering

The wavevector dependence of the diffuse scattering around the $(2.5\,0\,\bar{2})$ F-point is shown for two different temperatures in figure 3 for scans along the $\Gamma\text{--}F$ direction (which is the [1 0 4] reciprocal lattice direction), and in figure 4 for the perpendicular direction. The data have been corrected for absorption and polarization.

The scattering shown in figure 3 consists of a broad Lorentzian component centred on the F-point (where $\xi = 2.5$), with wings of rapidly increasing intensity on either side extending up to the Γ-points $(2\,0\,\bar{4})$ and $(3\,0\,0)$. This diffuse scattering behaves with the expected k^{-2} wavevector dependence (where the reduced wavevector $k = 0$ at the Γ-points), weighted with the respective zero-phonon structure factors of $(2\,0\,\bar{4})$ and $(3\,0\,0)$. Hence, each profile was fitted with a Lorentzian peak (for the F-point diffuse scattering), together with a weighted k^{-2} function for the wings, and a flat background which was also allowed to vary.

A narrow Bragg-like component centred on the F-point is also present in the data, which is due to $\lambda/2$ scattering from the $(5\,0\,\bar{4})$ Bragg peak. This scattering is transmitted by

the detector and analyser but not adequately discriminated against by the energy resolution of the detector. Below 512 K, where this scattering is quite strong, a Gaussian peak centred on the F-point was included in the fit. The value of χ^2 for each fit was generally found to be close to 1.0. The fitted lineshapes are shown as full curves in figure 3.

The scattering for the perpendicular direction—shown in figure 4—primarily consists of a Lorentzian peak centred on the F-point, with a gently sloping background due to the tail of the $(4\,0\,\bar{8})$ Bragg peak. This scattering did not follow the k^{-2} wavevector dependence as in the Γ–F scans, but instead was found to be fitted best with the somewhat arbitrary dependence of k^2. However, the fits obtained were never as satisfactory as those for the Γ–F scans, and the value of χ^2 was generally of the order of 2.0, which was also partly due to a small amount of extraneous diffuse scattering around $\xi = 1.75$ from the tail of the $(2\,0\,2)$ Bragg peak. The $\lambda/2$ scattering was ignored when fitting these scans, as the step size was twice as coarse as in the Γ–F scans, and hence was almost entirely missed by the diffractometer.

The width (FWHM) of the diffuse scattering associated with the F-point, as obtained from the Lorentzian fits, is shown in figure 5 for both the Γ–F scans and the perpendicular scans in units of Å^{-1}. For comparison, the Γ–F distance at 295 K is $0.16\,\text{Å}^{-1}$. The convention used here is that the reciprocal lattice distance associated with a lattice spacing of $d\,\text{Å}$ is $1/d\,\text{Å}^{-1}$. It is clear that the width of the scattering in the Γ–F direction steadily decreases as the temperature is increased, while for the perpendicular direction the width appears to be independent of temperature. As the width of the scattering along the Γ–F direction is somewhat greater than along the perpendicular direction, the scattering takes the form of a ridge joining Γ-points, as was also observed by Schmahl [16] and Shinnaka [17]. This is evidently due to the very flat dispersion of the soft acoustic branch along this direction, as shown in figure 2. As the temperature increases the dispersion becomes less flat because the branch softens around the F-point, and the width of the observed x-ray diffuse scattering decreases.
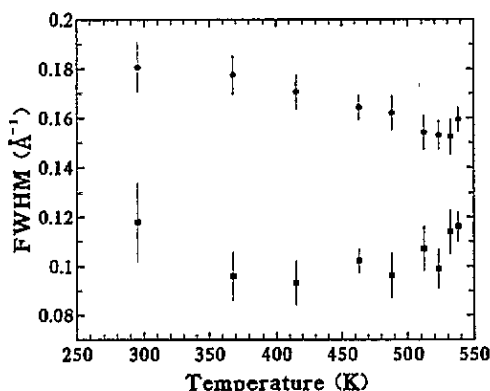

Figure 5. The temperature evolution of the fitted width (FWHM) of the F-scattering at the $(2.5\,0\,\bar{2})$ F-point for the Γ–F scans (filled circles), and for the perpendicular scans (filled squares).
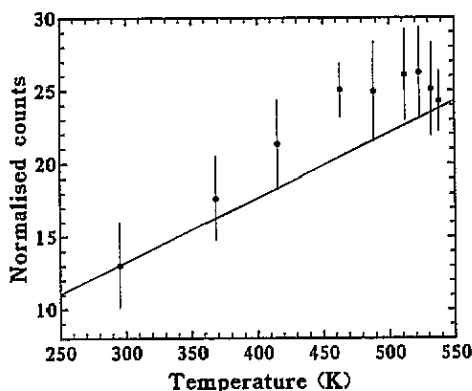
Figure 6. The peak height of the F-scattering shown as a function of temperature. The straight line through the lowest-temperature data point also intersects the origin and illustrates schematically the expected behaviour for a phonon intensity following Bose–Einstein statistics in the high-temperature limit. The partial deviation of the higher-temperature data from this behaviour represents evidence for softening.

Figure 6 shows the peak intensity of the diffuse scattering at the F-point as extracted from the fitting procedure. Also shown is a straight line through the origin and the room temperature data point, which represents the expected temperature-dependence for a phonon following Bose–Einstein behaviour. The data appear to deviate slightly above this behaviour as the temperature rises, presumably reflecting the increasing softening of the F-point phonon. Above about 500 K, however, the data seem to be approximately temperature-independent.

It is known from the inelastic neutron scattering work on $NaNO_3$ that the transverse acoustic branch softens from approximately 8 to 3 meV between 300 and 550 K [11–13]. This should result in the intensity of the diffuse x-ray scattering which is shown in figure 6 diverging with increasing temperature, rather than saturating above about 500 K. However, it is also known from ^{23}Na NMR experiments [21, 22] that the Na^+ ions undergo large-scale oscillations with increasing temperature, becoming especially prominent above about 470 K. The result is that the Na^+ Debye–Waller factor must increase significantly. Also, the atomic scattering factor of sodium ($Z = 11$) is somewhat larger than those of nitrogen ($Z = 7$) and oxygen ($Z = 8$) atoms, which effectively amplifies the effect as far as x-ray scattering is concerned. In addition, the Debye–Waller factors for the oxygen atoms also increase rapidly with temperature, due to the increasing nitrate group disorder. As can be seen from expression (4), these factors cause a decrease in the one-phonon structure factor with temperature so that above about 470 K the x-ray scattered intensity from a non-soft phonon at a general point in reciprocal space should fall away from the expected linear temperature-dependence. At the F-point, as the acoustic branch is soft here, the observed scattering must be the balance between the diverging susceptibility and the Debye–Waller factors. Figure 6 clearly shows that the Debye–Waller factors have the greater effect in this case for temperatures greater than 500 K.

The F-point scattering due to the soft branch is elliptical in reciprocal space [16, 17], with the major and minor axes given by the perpendicular measured widths of the scattering. The total integrated intensity of the scattering at each temperature was calculated, therefore, and is shown in figure 7. These data show a linear temperature-dependence, and the line shown in figure 7 is the result of a straight-line fit constrained to extrapolate to zero scattering intensity at 0 K (χ^2=1.16). This implies that the dominant temperature-dependent process for the scattering from the phonons around the F-point is simply high-temperature Bose–Einstein statistics. The diverging susceptibility and Debye–Waller factors appear to balance each other out around the F-point, which leaves the weaker Bose–Einstein dependence of the phonons to dominate.
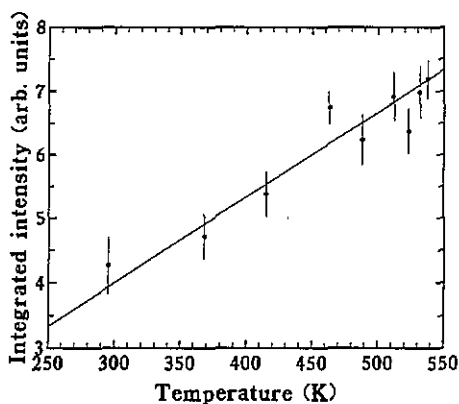

Figure 7. The total integrated intensity of the F-point scattering at (2.5 0 $\bar{2}$), shown as a function of temperature. The full line represents a linear fit through the origin.

4. Discussion

Inelastic neutron scattering measurements of calcite have shown the presence of a column of scattering at the F-point. This is associated with a softening transverse acoustic mode at the F-point, so that the column extends in energy from zero up to the the the soft-mode minimum [14, 15]. Over the temperature range 300–773 K, the energy-integrated intensity of the F-point scattering increases with temperature much more rapidly than would be expected from the usual linear high-temperature Bose–Einstein behaviour, and instead is more accurately described using an Arrhenius relation. This implies that the column of scattering is due to a thermally-activated process. A possible candidate for this process is the formation of clusters of a phase with a structure based on the F-point symmetry, with space group $P2/a$. In this ordering scheme, anions in planes perpendicular to the Γ–F direction have the same orientation, with successive planes having the opposite orientation. This is incompatible with the conventional Z-point ordering scheme, where the orientation of anions is identical in the planes perpendicular to the c-axis [8].

In $NaNO_3$ the situation seems to be rather different, despite the fact that both $NaNO_3$ and calcite are isomorphous, and have an identical symmetry change at their phase transitions. As has already been discussed, inelastic neutron scattering measurements [11–13] show that the transverse acoustic branch softens at the F-point in $NaNO_3$, which is in common with calcite. As an aside it should be emphasized that, as this softening takes place in what are both essentially order-disorder systems, its origins are not at present clear. However, unlike the case of calcite, the branch has a very flat dispersion around the F-point, except at temperatures above about 500 K, where the branch starts to dip down towards zero energy at the F-point (figure 2). Furthermore, no sharp column of anomalous scattering is observed in $NaNO_3$, but instead a rather different—but equally unusual—phenomenon occurs. This phenomenon takes the form of a broad swathe of diffuse inelastic scattering around the F-point which lies underneath the acoustic modes but extends to much higher energies [12]. It is broad in both energy and wavevector transfer, with widths (FWHM) of approximately 25 meV and 0.4 $Å^{-1}$ respectively. The origin of this scattering is not fully understood at present, and it is not known how, or if, it is related to the inelastic column in calcite. Unfortunately, owing to its apparently small temperature-dependence and extreme diffusivity, the swathe of scattering could not be detected above the effects of the transverse acoustic branch in the x-ray results presented here.

Returning to the soft branch in $NaNO_3$, Schmahl and co-workers [11] have measured the temperature-dependence of the F-point soft phonon and extracted the dynamic pair correlation function. Using their results, together with the observations of the x-ray diffuse scattering reported here, it is possible to partially determine the eigenvectors of the soft mode at the F-point. The static pair correlation function was calculated for each observed temperature by integrating the $S(\omega)$ given by Schmahl and co-workers with respect to ω. Using (1) and (2) and the $NaNO_3$ Debye–Waller factors of Paul and Pryor [23], this enabled $Q \cdot e_n(q = 0)$ with $Q = [2.5\,0\,\bar{2}]$ to be determined for each atom type by a fitting procedure incorporating the data for each observed temperature ($\chi^2 = 1.42$). The results for the eigenvectors are

$$2.5e_{Na}^x - 2e_{Na}^z = -0.8 \pm 0.1 \tag{7}$$

$$2.5e_{N}^x - 2e_{N}^{\bar{z}} = -1.15 \pm 0.07 \tag{8}$$

$$2.5e_{O}^x - 2e_{O}^z = -0.04 \pm 0.05 \tag{9}$$

where the a and c components of the eigenvector for each atom n are e_n^x and e_n^z, respectively. Results (7) and (8) suggest that the motions of the sodium and nitrogen atoms for the F-point phonon involve a large component parallel to the c-axis (compared to that along the a axis). For the oxygen atoms, $Q \cdot e_O(q = 0) \approx 0$, so that

$$\frac{e_O^z}{e_O^x} \approx \frac{2.5}{2} = 1.25. \tag{10}$$

One possibility is that the a and c-components of motion of the oxygen atoms in the F-point soft mode are close in magnitude. The formation of the proposed F-structure from the Z-structure necessitates strong translation–rotation coupling so that 60° rotations of nitrate groups in the a–c plane of the Z-structure occur simultaneously with translations. Result (10) suggests that in the formation of the F-structure, the nitrate group translation may involve a component in the a–c plane together with a component out of the plane which is of a similar magnitude.

However, this analysis has necessarily assumed that the soft mode treats all of the oxygen atoms identically, and hence an alternative explanation for result (10) could be that the soft mode involves differential motions for each oxygen atom in the unit cell. These motions could then very nearly cancel each other out upon addition, so that $Q \cdot e_O(q = 0) \approx 0$. Hence, it is unnecessary to invoke a large component of the eigenvector parallel to the c axis to explain result (10). Unfortunately, it is impossible to distinguish from the experimental data between this and the previous interpretation for the motion of the oxygen atoms, but it certainly seems likely that the sodium and nitrogen atoms undergo large-scale oscillations out of the a–c plane due to the F-point soft mode. This alone suggests that the eigenvectors for the oxygen atoms may involve a similar component.

In conclusion, the x-ray diffuse scattering at the F-point in NaNO$_3$ behaves largely as that expected from an acoustic branch. This branch has been observed to soften in neutron scattering experiments, but rapidly increasing x-ray Debye–Waller factors prevent the intensity of the scattering from diverging on heating as would otherwise be expected. The process which is responsible for the softening is not a thermally activated process which may be described by simple Arrhenius statistics, as it can be in calcite. The diffuse scattering cannot be considered as a form of critical scattering, where the width is an indication of the correlated size of ordered clusters. Instead, the scattering width merely reflects the degree of softening of the transverse acoustic branch around the F-point. It is apparent that the width of the scattering is different in the Γ–F and perpendicular directions, such that the scattering takes the form of a ridge between Γ-points. This indicates that the dispersion of the transverse acoustic branch around the F-point is considerably steeper in the perpendicular direction compared to that along Γ–F. This in turn implies that the structure is softer to the phonon eigenvectors along the Γ–F direction. So far, this softening has been linked with the formation of the hypothetical F-phase with space group $P2/a$ (which essentially involves an order–disorder process), but it is not clear exactly how this results in the soft mode. The same is true for calcite, and satisfactory mechanisms have yet to be established for both compounds.

References

[1]   Chisler E V 1969 *Sov. Phys.–Solid State* **11** 1032
[2]   Brooker M H 1978 *J. Phys. Chem. Solids* **39** 657
[3]   Neumann G and Vogt H 1978 *Phys. Stat. Solidi* (b) **85** 179
[4]   Poon W C-K 1988 Raman and birefringence studies of phase transitions *PhD thesis* University of Cambridge
[5]   Fontana M D, Brehat F and Wyncke B 1990 *J. Phys.: Condens. Matter* **2** 9125
[6]   Brehat F and Wyncke B 1985 *J. Phys. C: Solid State Phys.* **18** 4247
[7]   Harris M J, Salje E and Güttler B K 1990 *J. Phys.: Condens. Matter* **2** 5517
[8]   Lynden-Bell R M, Ferrario M, McDonald I R and Salje E 1989 *J. Phys.: Condens. Matter* **1** 6523
[9]   Poon W C-K and Salje E 1988 *J. Phys. C: Solid State Phys.* **21** 715
[10] Schmahl W W and Salje E 1989 *Phys. Chem. Minerals* **16** 790
[11] Schmahl W W, Pintchovius L and Fuess H 1989 *Zeit für Krist* **186** 261
[12] Harris M J, Hagen M E, and Dove M T 1993 *J. Phys.: Condens. Matter* (to be submitted)
[13] Harris M J 1991 Phase transitions in related ionic nitrates and carbonates *PhD Thesis* University of Cambridge
[14] Dove M T, Hagen M E, Harris M J, Powell B M, Steigenberger U and Winkler B 1992 *J. Phys.: Condens. Matter* **4** 2761
[15] Hagen M, Dove M T, Harris M J, Steigenberger U and Powell B M 1992 *Physica* B **180–181** 276
[16] Schmahl W W 1988 (unpublished)
[17] Shinnaka Y 1964 *J. Phys. Soc. Japan* **19** 1281
[18] Brunet F, McMorrow D F, Gibaud A, and Patterson C 1990 *J. Phys.: Condens. Matter* **2** 10549
[19] Reeder R J, Redfern S A T and Salje E 1988 *Phys. Chem. Minerals* **15** 605
[20] Bruce A D and Cowley R A 1981 *Structural Phase Transitions* (London: Taylor and Francis)
[21] Andrew E R, Eades R G, Hennel J W and Hughes D G 1962 *Proc. Phys. Soc.* **79** 954
[22] D'Alessio G J and Scott T A 1971 *J. Magn. Res.* **5** 416
[23] Paul G L and Pryor A W 1972 *Acta. Cryst.* B **28** 2700